carbonyls. If the difference between the internal five- and six-membered rings of OPA is approximated to be 0.75 log unit, this means that 15% of the chelate would have a six-membered ring structure and 85% would have the five-membered ring structure.

Proton NMR measurements[25] using Eu(III) in unspecified concentrations have shown that oxaloacetic acid complexes of the ML^+ type preferably form five-membered chelate rings. The half-life of Eu^{3+}–OAA chelates should be slightly under 3 min on the basis of values obtained for La(III) and Gd(III).[34] Solutions having 1:1 molar ratios of ligand to metal ion at concentrations high enough for the observation of NMR resonances of metal chelates have significant concentrations of the chelates and therefore exhibit considerable catalytic activity. The time required to obtain an initial NMR measurement of the Eu(III)–OAA system is close to the half-life of decarboxylation of the complex. The fact that niether the existence of the hydrate species[35] nor the increase in the amount of enol species in solution in the presence of metal ions[14,15,22] is detected casts some doubt upon the conclusions made in the earlier NMR study. Given a 10% error under these conditions as well as the fact that half the substrate has already decomposed, it appears that initially there may be as much as 20% of an undetected species. Covey and Leussing[14] in their work with OAA came to the same conclusion and suggested the seven-membered ring instead of the six-membered ring to account for the high stabilities of OAA complexes compared to those of pyruvate. This is in accord with the stability of the seven-membered chelate ring of the zinc(II)–succinate complex ($10^{1.76}$).[34] Their explanation does not consider the adverse inductive effect on the stability constant resulting from a carbonyl adjacent to one of the carboxylates (**3**). It is thought the inductive effect is sizable since an adjacent carbonyl has a large effect on the pK_a of the carboxyl. The difference in the pK_as of propanoic (4.67)[31] and pyruvic acids (2.23)[31] at 25 °C and 0.10 M ionic strength is 2.41 log units while the change in the proton association constants of butanoic (4.63)[31] and α-ketobutyric acids (2.48) is 2.15 log units. On this basis it is estimated the stability constants of Zn(II)–OAA^{2-} and Zn(II)–OPA^{2-} seven-membered chelates have values well under 10. However, it is believed the log (stability constant) of the six-membered Zn(II)–OPA^{2-} chelate (**2**) is well over 1 log unit. It may be argued that the OPA cis-enol seven-membered ring, **3a**, adds to the stability of the seven-membered chelate, but this is doubtful. A CPK molecular model of this species, **3a**, indicates the negatively charged oxygens of both carboxylates come in close contact with each other, resulting in instability because of electrostatic repulsions. The model also demonstrates there is no available space that a metal ion could occupy to stabilize the negative charges on the carboxylates. Also, it is not reasonable to expect the molecule to bend or twist to accommodate a metal ion because of the planarity of the conjugated system and the existence of a hydrogen bond between the hydroxyl and the carbonyl of the adjacent carboxylate. For the reasons stated it is proposed that the five-membered ring is the major chelate species and the six-membered ring is the minor chelate species in OPA- and OAA-metal ion systems, with the seven-membered ring making little or no significant contribution to the solution chemistry.

Acknowledgment. This work was supported by a research grant, No. AM-11694, from the National Institute of Arthritis, Metabolism and Digestive Diseases, U.S. Public Health Service.

Registry No. OPA, 642-93-3; AAA, 541-50-4; AKBA, 600-18-0; Zn, 7440-66-6; Al, 7429-90-5; Cu, 7440-50-8.

Contribution from the Sonderforschungsbereich 127 der DFG (Kristallstruktur und chemische Bindung) and Fachbereich Chemie, Universität Marburg, 3550 Marburg, West Germany

High-Spin–Low-Spin Equilibria of Cobalt(2+) in the Terpyridine Complexes $Co(terpy)_2X_2 \cdot nH_2O$

S. KREMER, W. HENKE, and D. REINEN*

Received December 8, 1981

For the complexes $Co(terpy)_2X_2 \cdot nH_2O$ with X = Cl^-, Br^-, I^-, NO_3^-, or ClO_4^- and different n values optical spectra, EPR resonances, and magnetic moments are measured between 300 and 4.2 K. From the temperature variation of the susceptibility for different X an equilibrium between the octahedral high-spin $^4T_1$ and low-spin ^2E states of the d^7 configuration can be deduced. The ligand field spectra show nearly exclusively doublet–doublet transitions independent of the high-spin/low-spin ratio. At low temperature EPR spectra of both spin states are observed side by side for X = ClO_4^- and are attributed to differently distorted Co^{2+} sites in the lattice. While the high-spin state seems to be stabilized by the "ligand effect" in combination with spin–orbit coupling, the low-spin **g** tensors indicate the presence of an additional, rather strong Jahn–Teller distortion. The "ligand effect" corresponds to a tetragonal compression of the CoN_6 octahedra as the consequence of the rigid structure of the terpyridine molecule. In the case of a low-spin ground state this distortion is superimposed by an elongation perpendicular to the direction of compression, which is induced by the Jahn–Teller effect. The low-spin ground state is stabilized with respect to the high-spin ground state by a strong vibronic Jahn–Teller coupling in the octahedral ^2E level. The spin exchange can be explained alternatively by an intermolecular, cooperative mechanism as well as by an intramolecular thermal spin equilibrium. The available structural, spectroscopic, and magnetic data are interpreted on the basis of the AO model, with use of the local and cooperative Jahn–Teller effect.

Introduction

The terpyridine complexes of transition-metal ions $T^{II}(terpy)_2X_2 \cdot nH_2O$ crystallize in tetragonal and triclinic structures, depending on the nature of the anion X and the water content n.[1-4] The two rigid tridentate ligands force upon the d^n cation a distorted octahedral coordination of approximate D_{2d} symmetry, the dominant characteristic of which is a

* To whom correspondence should be addressed at the Fachbereich Chemie, Universität Marburg, 3550 Marburg, West Germany.

(1) E. N. Maslen, C. L. Raston, and A. H. White, *J. Chem. Soc., Dalton Trans.*, 1803 (1974).
(2) R. Allmann, W. Henke, and D. Reinen, *Inorg. Chem.* **17**, 378 (1978).
(3) W. Henke and S. Kremer, *Inorg. Chim. Acta*, in press.
(4) R. Allmann, W. Henke, and D. Reinen, *Proc. Int. Conf. Coord. Chem., 21st*, 33 (1980); W. Henke, R. Allmann, S. Kremer, and D. Reinen, to be submitted for publication.

0020-1669/82/1321-3013$01.25/0

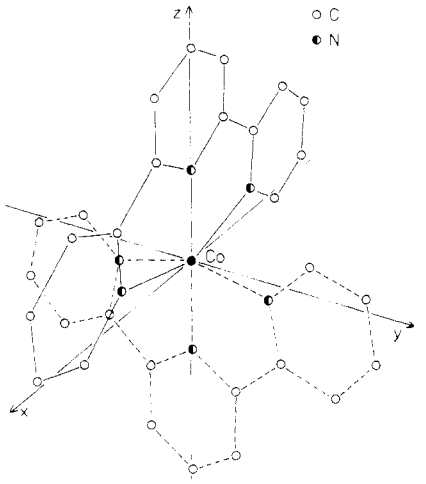

Figure 1. Geometry of $T(terpy)_2^{2+}$ polyhedra in the compounds $T^{II}(terpy)_2X_2 \cdot nH_2O$ (though the equatorial T–N bond lengths are bent with respect to the molecular (001) plane, they will be correlated with the x and y directions in the text for the sake of a simplified description).

compression along the molecular z axis (Figure 1). In the case that T^{II} is a Jahn–Teller unstable cation with an electronic E ground state in octahedral coordination, as Cu^{2+} for example (strong vibronic coupling $E \otimes \epsilon$ case[5]), an *elongation* along the x or y direction perpendicular to z is superimposed, which leads to CuN_6 polyhedra of C_{2v} symmetry.[2,6]

The cooperative Jahn–Teller order is antiferrodistortive[5] in the tetragonal structures[2] and ferrodistortive[5] if the complexes crystallize in a triclinic space group.[4] At higher temperatures the Jahn–Teller-induced symmetry component is dynamic, however, with equal equatorial Cu–N bond lengths in time average in the high-temperature modifications. Similar results are expected for low-spin Co^{2+} ($t_2^6e^1$—^2E ground state).

With use of the ligand field and EPR spectroscopic results on $Cu(terpy)_2(NO_3)_2$[6] within a complete crystal field calculation in C_{2v} the parameter set of Table I is obtained. The angular distortion parameter φ_0 deduced from the **g** tensor is identical with the one calculated from the Cu–N bond lengths by the equation

$$\varphi_0 = \arctan\left(3^{1/2}\frac{\Delta x - \Delta y}{2\Delta z - \Delta x - \Delta y}\right) \quad (1)$$

The radial distortion parameter is defined by

$$\rho_0 = (\sum 2(\Delta i)^2)^{1/2} \quad (2)$$

($a_i = \bar{a} + \Delta i$ with $i = x, y, z$ and $3\bar{a} = a_x + a_y + a_z$). The linear Jahn–Teller coupling parameter V_ϵ and the force constant of the radial vibration $M\omega_\epsilon^2$ can then be calculated, with use of the Jahn–Teller splitting of the ^2E ground state ($\equiv 4E_{JT}$):

$$E_{JT} = \tfrac{1}{2}\rho_0|V_\epsilon| \qquad \rho_0 = |V_\epsilon|/M\omega_\epsilon^2 \quad (3)$$

With an atomic weight of 78 as the approximate mass of one ligand the energy of the radial ϵ vibration is roughly 120 cm^{-1}.

In the "angular overlap model" (AOM[7]) the Jahn–Teller energy is as follows (D_2 symmetry of CuN_6 polyhedra):

$$E_{JT}(^2E) = \tfrac{1}{2}(\sum_i (e_\sigma^i)^2 - \tfrac{1}{2}\sum_{i\neq j} e_\sigma^i e_\sigma^j)^{1/2} \quad (4)$$

($e_\sigma^i = K_\sigma(S_\sigma^i)^2$; $i, j = x, y, z$; S_σ = standard overlap integral).

Table I. Observed and Calculated Ligand Field Transitions (in cm^{-1}) and g Values and Calculated Ligand Field and Distortion Parameters for $Cu(terpy)_2(NO_3)_2$ (C_{2v} Symmetry, Including LS Coupling ($\lambda_0 = 823$ cm^{-1}); 298 K)

	$g_{x(y)}$	$g_{y(x)}$	g_z	$^2a_1 \rightarrow {}^2b_1$	$^2A_2$[a]	$^2B_1$, $^2B_2$
obsd	2.25_8	2.09_9	2.03_7	6.5_5		14.7
calcd	2.26_1	2.09_4	2.03_4	6.6	13.6	14.5, 15.1

	Δ_0[b]	E_{JT}	E_{JT}'[c]	ρ_0, pm	φ_0, deg	k[d]	$\lvert V_\epsilon\rvert$, cm^{-1} pm^{-1}	$M\omega_\epsilon^2$, cm^{-1} pm^{-2}
calcd	11.0	1.65	≃0.3	30.5	136, 224	0.87	108	3.5

	e_σ^x	e_σ^y	e_σ^z	e_π^x	e_π^y	e_π^z
calcd	3.4	5.8	7.4	0.8	1.8	2.6

[a] Symmetry forbidden in C_{2v}. [b] Δ_0 is the octahedral ligand field parameter ($\equiv \frac{1}{3}(E(^2a_1 \rightarrow {}^2A_2) + E(\rightarrow {}^2B_1) + E(\rightarrow {}^2B_2) - \frac{1}{2}E(\rightarrow {}^2b_1)$). [c] Estimated from AOM calculations. [d] k is the covalency parameter ($k_x \simeq k_y \simeq k_z$) defined by $\lambda = k_i^2\lambda_0$, $i = x, y, z$ (λ_0 = spin–orbit coupling parameter of the free ion).

The angular distortion parameter φ_0 is accessible in the framework of this model as well:

$$\varphi_0^*(^2E) = \arctan\left(3^{1/2}\frac{e_\sigma^x - e_\sigma^y}{2e_\sigma^z - (e_\sigma^x + e_\sigma^y)}\right) \quad (5)$$

Provided that the e_σ^i change linearly with the bond lengths, dS^2/da = constant, φ_0 and φ_0^* are identical. The expression given by Bacci[8] for calculating V_ϵ from AOM parameters

$$|V_\epsilon| = \frac{3^{1/2}}{2}K_\sigma\left(\frac{\delta S_\sigma^2}{\delta a}\right)_{\bar{a}} \quad (6)$$

is equivalent to eq 4.

Expressions analogous to the $E \otimes \epsilon$ coupling case can be derived for the linear vibronic $T \otimes \epsilon$ coupling in the excited $^2T_2$ level. The equations corresponding to (4) and (5) for the $T \otimes \epsilon$ coupling case are (Cu^{2+}, excited-$^2T_2$-state splitting $3E_{JT}'$)

$$E_{JT}' = \tfrac{1}{2}\rho_0'|V_\epsilon'| = \tfrac{2}{3}(\sum_i (e_\pi^i)^2 - \tfrac{1}{2}\sum_{i\neq j} e_\pi^i e_\pi^j)^{1/2} \quad (4a)$$

$$e_\pi^i = K_\pi(S_\pi^i)^2$$

$$\varphi_0' = \arctan\left(3^{1/2}\frac{e_\pi^x - e_\pi^y}{2e_\pi^z - (e_\pi^x + e_\pi^y)}\right) \quad (5a)$$

In the case of $Cu(terpy)_2^{2+}$ cations, where the Cu–N π bonding within the planes of the terpyridine rings has to be assumed to be zero (Figure 1), the following simplified expression results (D_2 symmetry):

$$E_{JT}' = \tfrac{1}{3}[e_\pi^z - 2(e_\pi^x + e_\pi^y)] \quad (4b)$$

Refining the model by taking into account the C_{2v} symmetry experimentally observed in compounds of this type, we obtain the AOM energies shown in (7). The calculation was based

$$\begin{aligned}
&^2A_1: \; E(d_{z^2}) = 0.35(e_\sigma^x + e_\sigma^y) + 2e_\sigma^z \\
&^2A_1: \; E(d_{x^2-y^2}) = 1.34(e_\sigma^x + e_\sigma^y) \\
&^2B_2: \; E(yz) = 0.31e_\sigma^y + e_\pi^z + 0.11e_\pi^x \\
&^2B_1: \; E(xz) = 0.31e_\sigma^x + e_\pi^z + 0.11e_\pi^y \\
&^2A_2: \; E(xy) = 1.89(e_\pi^x + e_\pi^y) \\
&\langle d_{z^2}|V|d_{x^2-y^2}\rangle = 0.69(e_\sigma^y - e_\sigma^x)
\end{aligned} \quad (7)$$

on an angle of ±13° between the equatorial N ligands and

(5) D. Reinen and C. Friebel, *Struct. Bonding (Berlin)*, **37**, 1 (1979). The terms "ferrodistortive" and "antiferrodistortive" are explicitly defined in the text (pp 14–17) and illustrated in Figures 8 and 9.
(6) W. Henke and D. Reinen, *Z. Anorg. Allg. Chem.*, **436**, 187 (1977).
(7) C. E. Schäffer, *Pure Appl. Chem.*, **24**, 361 (1970).
(8) M. Bacci, *Chem. Phys. Lett.*, **58**, 537 (1978).

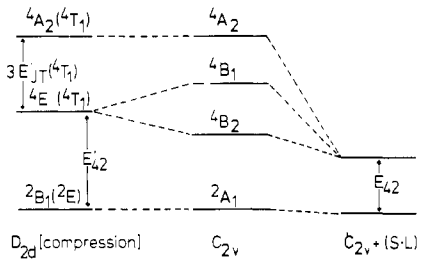

Figure 2. Qualitative energy diagram of the competing lowest high-spin and low-spin states of Co^{2+} (for C_{2v} + (L·S) only the two lowest energy Kramers doublets out of seven are shown).

the xy plane (Figure 1). The specific orientation of the ligand rings leads to a split level A_2 of the octahedral parent T_2 state, which is stronger π antibonding than B_1 and B_2. For $e_\sigma^{xy}/e_\pi^{xy} \lesssim 7$ the energy sequence of these levels is independent of the sign of distortion (compression or elongation). From the experimental ground-state splitting $4E_{JT}$ the transition energies $^2_aA_1 \rightarrow {}^2B_1$, $^2B_2$ and the Cu–N bond lengths in $Cu(terpy)_2(NO_3)_2$[2], K_σ and K_π values (defined in eq 4 and 4a) of 1.47 × 10^6 and 1.54 × 10^6 cm^{-1} are derived. Atomic functions of $Cu^{2+}(3d)$ and $N^0(2p)$[9] were used to calculate the overlap integrals. The calculated band positions including LS coupling are in good agreement with the experimental transitions (Table I). The observation of only one broad band at 14 700 cm^{-1} is expected because the electric dipole moment for the $^2_aA_1 \rightarrow {}^2A_2$ transition vanishes.

If Co^{2+} is the transition-metal ion in terpyridine complexes of the type considered, magnetic measurements give hints for a thermal equilibrium between low-spin and high-spin states.[10,11] While a σ-antibonding ^2E ground state should be strongly Jahn–Teller unstable in close analogy to Cu^{2+}, the alternative $^4_aT_1$ ground state is derived mainly from the π-antibonding $t_2^5e^2$ configuration and is not expected to exhibit larger Jahn–Teller splittings. The energy difference between the two competing levels—for the general case of a compressed CoL_6 octahedron and without LS coupling and nondiagonal elements of the tetragonal energy matrix (D_{2d})—is of the magnitude

$$E_{42}' \cong \Delta_0 - 4B - 4C + 2E_{JT} - E_{JT}' \qquad (8)$$

or, if one distinguishes between the ligand field parameters in the high- and low-spin states:

$$E_{42}' \cong 1.8\Delta_0(^2E) - 0.8\Delta_0(^4T_1) + 8B(^2E) - 12B(^4T_1) - 4C(^2E) + 2E_{JT}(^2E) - E_{JT}'(^4T_1) \qquad (9)$$

Because Co^{2+} is significantly larger in the high- (r_4 = 73.5 pm) than in the low-spin state (r_2 = 65 pm),[12] the relations $\Delta_0(^2E) > \Delta_0(^4T_1)$ and $B,C(^2E) < B,C(^4T_1)$ are expected to be valid. The "crossover" situation corresponds to $E_{42}' = 0$.

A qualitative energy level diagram for compressed D_{2d} and orthorhombic C_{2v} symmetries (low-spin ground state and the $^4_aT_1$ split levels slightly higher in energy) is shown in Figure 2. The energy separation E_{42} is a function of all LF parameters including LS coupling.

The extension of the LF model by taking the vibronic coupling explicitly into account—again for the D_{2d} symmetry of compressed CoN_6 polyhedra—leads to the following adiabatic potentials of the competing energetically lowest $^2B_1$ (^2E) and ^4E ($^4T_1$) states:

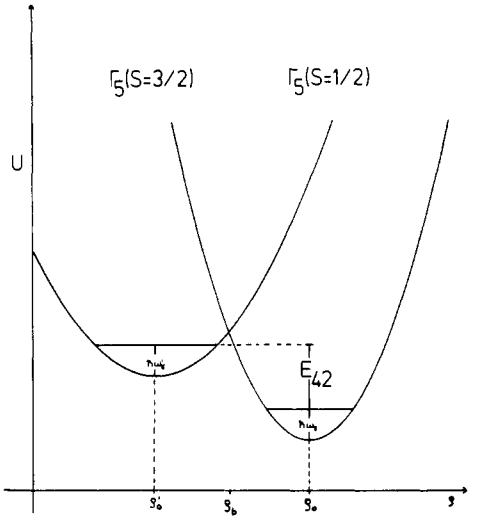

Figure 3. Adiabatic potentials of the two lowest energy Kramers doublets in C_{2v} symmetry including LS coupling (compare Figure 2).

$$U(^2B_1) = -1.8\Delta_0(^2E) - 8B(^2E) + 4C(^2E) + \tfrac{1}{2}M\omega_\epsilon^2\rho_0^2 - |V_\epsilon|\rho_0$$

$$U(^4E) = -0.8\Delta_0(^4T_1) - 12B(^4T_1) + \tfrac{1}{2}M\omega_\epsilon'^2\rho_0'^2 - \tfrac{1}{2}|V_\epsilon'|\rho_0' \qquad (10)$$

The energy barrier at ρ_b, which controls the thermal equilibrium between the lowest high- and low-spin states, is depicted in Figure 3. If one adds the zero-point energies of the radial vibrations $\hbar\omega_\epsilon$ and $\hbar\omega_\epsilon'$ to eq 10 and includes LS coupling, the high-spin–low-spin separation E_{42} is defined as the energetic difference between the vibrational zero-point levels of the two potential curves.

The special case of the $Co(terpy)_2^{2+}$ cation with restricted π-bonding possibilities, as discussed already for Cu^{2+}, is treated in detail below. Though we have distinguished between a "ligand effect" (D_{2d}, compression) and an additional "Jahn–Teller symmetry component" ($D_{2d} \rightarrow C_{2v}$) in the beginning of this section for the sake of a clear demonstration, the calculation treats the deviation from octahedral O_h symmetry as only one (vibronically induced) effect.

The results of spectroscopic, magnetic, and structural investigations on the terpyridine complexes $Co(terpy)_2X_2 \cdot nH_2O$ will demonstrate that high-spin–low-spin equilibria of d^7-configured cations in octahedral coordination are strongly influenced by the considerable Jahn–Teller stabilization energy, which is connected with the lowest low-spin ^2E level. An effect of this kind was found to stabilize the low-spin configuration of Ni^{3+} in ordered perovskites $A_2A'Ni^{III}F_6$ (A, A' = alkaline cations) for example—with a quartet–doublet separation of only several hundred wavenumbers—while the corresponding Co^{3+} compounds are of the high-spin type.[5,13] A short preliminary report on the subject of this paper has already been given elsewhere.[14]

Experimental Section

Preparation of Complexes $Co(terpy)_2X_2 \cdot nH_2O$. The salt CoX_2 is treated with a small excess of terpyridine in boiling aqueous solution. Slow evaporation of the solution at room temperature leads to crystallization. If CoX_2 is not available, KX is added to the solution containing $CoCl_2$ and terpyridine.

1. X = Cl⁻, n = 5. Black plates, extremely well soluble in water, were obtained. Anal. Calcd: C, 51.49; N, 12.24; H, 4.70. Found:

(9) J. W. Richardson, W. C. Nieuwpoort, R. R. Powell, and W. F. Edgell, *J. Chem. Phys.*, **36**, 1057 (1962); F. Clementi, *ibid.*, **40**, 1944 (1964). For Cu^{2+} and Co^{2+} the resulting e_σ and e_π parameters give a more reasonable description of the metal to ligand bonds than those based on the more frequently used monovalent cations. The reason may be seen in the semiempirical nature of the model.

(10) J. S. Judge and W. A. Baker, *Inorg. Chim. Acta*, **1**, 68 (1968).

(11) D. L. Williams, D. W. Smith, and R. C. Stoufer, *Inorg. Chem.*, **6**, 590 (1967).

(12) R. D. Shannon and C. T. Prewitt, *Acta Crystallogr., Sect. B*, **B25**, 925 (1969).

(13) D. Reinen, C. Friebel, and V. Propach, *Z. Anorg. Allg. Chem.*, **408**, 187 (1974).

(14) S. Kremer and D. Reinen, *Proc. Int. Conf. Coord. Chem., 21st*, 485 (1980).

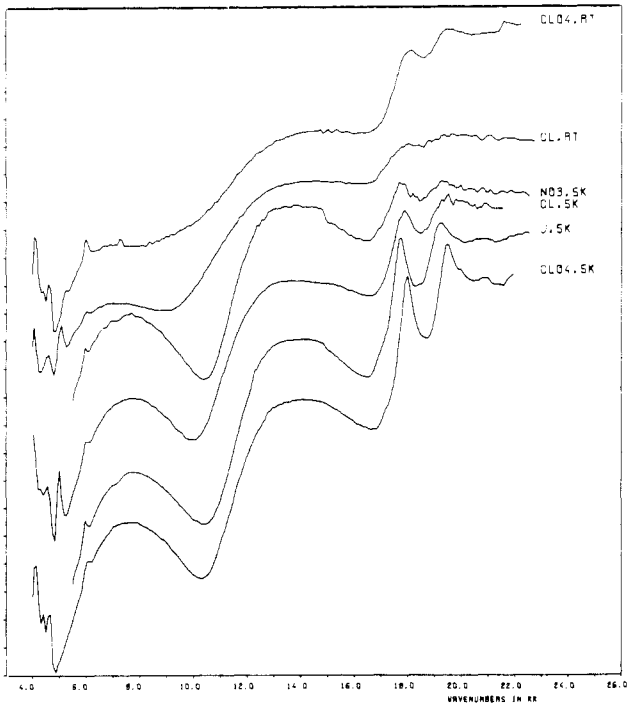

Figure 4. Reflection spectra of the compounds $Co(terpy)_2X_2 \cdot nH_2O$ (for n see text) at 300 and 5 K (fine structure at $\bar{\nu} \lesssim 6000$ cm^{-1} is caused by the terpyridine ligand;[6] extinction is given in 0.1-unit increments of log k/s with the scale shifted for each spectrum).

C, 52.0; N, 12.2$_5$; H, 4.2. Drying the crystals over P_2O_5 reduces the water content to $n = 1.5$. Anal. Calcd: C, 58.15; N, 13.48; H, 4.04. Found: C, 57.9; N, 13.9; H, 3.8$_5$.

2. X = Br$^-$, $n = 3$. Brown plates were obtained. Anal. Calcd: C, 48.74; N, 11.37; H, 3.82. Found: C, 48.5$_5$; N, 11.4$_5$; H, 3.2$_5$.

3. X = I$^-$, $n = 1.5$. Black quadratic pyramids were obtained. Anal. Calcd: C, 44.69; N, 10.44; H, 3.13. Found: C, 44.5; N, 10.4$_5$; H, 2.8$_5$.

4. X = NO_3^-, $n = 0.5$. Brown plates were obtained. Anal. Calcd: C, 54.72; N, 17.02; H, 3.52. Found: C, 54.7$_5$; N, 16.8; H, 3.3$_5$.

5. X = ClO_4^-, $n = 0.5$. Red transparent crystals of pyramidal shape were obtained. Anal. Calcd: C, 49.19; N, 11.46; H, 3.16. Found: C, 49.0; N, 11.4; H, 3.1.

Spectroscopic and Magnetic Measurements. The diffuse-reflection spectra between 4×10^3 and 25×10^3 cm^{-1} at 298 and 5 K as well as the solution spectra in H_2O and CH_3OH have been recorded by a Zeiss spectrophotometer, Model PMQ II (with a low-temperature accessory).

The EPR single-crystal and powder measurements between 298 and 4.2 K were performed with a Varian E 15 spectrometer at the X- and Q-band frequencies.

A Foner magnetometer with a cryostat was used for taking the magnetization data between 4.2 and 298 K (calibration with Hg[Co(NCS)$_4$]).

Structural Data. The compounds with X = ClO_4^-, $n = {}^1/_2$,[3] and X = NO_3^-, $n = {}^1/_2$, crystallize in the tetragonal space group $I4_1/a$ and are isostructural with $Cu(terpy)_2(NO_3)_2$.[2] For X = Br, $n = 3$, a triclinic unit cell of space group $P\bar{1}$ was found.[1,4] The local symmetry of the CoN_6 polyhedra in these complexes at 298 K is fairly well described by tetragonally compressed octahedra of symmetry C_{2v} with an angle of $\lesssim 13°$ between the equatorial Co–N bonds and the xy plane (Figure 1).

Results

Ligand Field Spectra. The reflection spectra of the crystal powders between 4×10^3 and 22×10^3 cm^{-1} (Figure 4) show two broad bands at $\simeq 7500$ and $\simeq 15\,000$ cm^{-1} with two additional sharper absorptions at 17 800 (±200) and 19 200 (±200) cm^{-1}. In solution the absorption maxima are found at 15 300 (ϵ 100), 18 200 (ϵ 450), 20 000 (ϵ 1300), and 22 500 (ϵ 1500) cm^{-1}. It is not clear whether the intense peaks at 18 200, 20 000, and 22 500 cm^{-1} are charge-transfer bands or

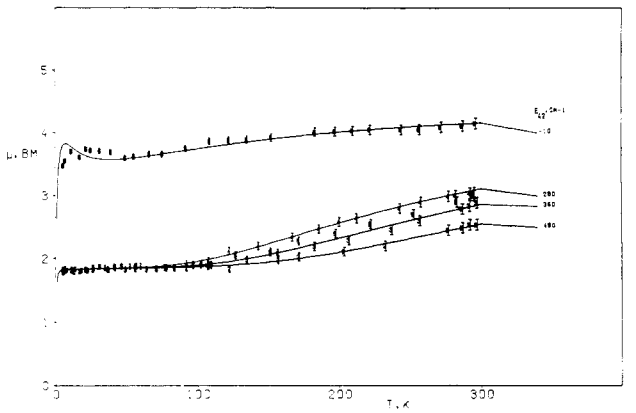

Figure 5. Experimental μ_{eff} values in dependence on T from susceptibility data for complexes $Co(terpy)_2X_2 \cdot nH_2O$. (X, n (from below): Cl$^-$, 5; Br$^-$, 3; I$^-$, 1.5; NO_3^-, 0.5; ClO_4^-, 0.5. Full curves are calculated with the indicated high-spin–low-spin energy separations E_{42} (except for I$^-$, 1.5).)

d–d transitions that are superimposed on the increase of extinction characterizing the beginning of the charge-transfer region. We could not detect the absorption band of lowest energy in Co^{2+} solutions—in contrast to the case for solutions of $Cu(terpy)_2^{2+}$ ions, in which the corresponding transition at 7500 cm^{-1} is well resolved. The reason may be either the much weaker intensity in the case of Co^{2+} or an energy shift into the region of solvent absorption ($\lesssim 7000$ cm^{-1}). It should be noted, however, that the band at 7500 cm^{-1} is distinctly present in the reflection spectra of $Co(terpy)_2^{+}$ cations (Figure 4) and has not been observed up to now.[11] EPR and susceptibility measurements indicate a ground state with predominant low-spin character for $Co(terpy)_2^{2+}$ in solution ($g_{eff} \approx 2.1$, μ_{eff}(300 K) $\approx 3.1\ \mu_B$). In the solid—in spite of the increasing population of the lowest quartet state in the sequence X = Cl$^-$, Br$^-$, I$^-$, NO_3^- (compare Figure 5)—the electronic spectra between 298 and 4.2 K are comparable. Even the ClO_4^- complex, with local Co–N distances suggesting predominantly high-spin Co^{2+} ions, shows essentially the same spectrum. Obviously the quartet–quartet transitions are hidden by the doublet–doublet excitations. This is supported by the much weaker band intensities in the ligand field spectra of typical high-spin complexes such as $Co(quaterpyridyl)(H_2O)_2^{2+}$, $Co(bpy)_3^{2+}$, and $Co(py)_6^{2+}$ with an extinction of $\epsilon \sim 10$.

The quantitative interpretation of the ligand field bands depends essentially on the assignment of the transition at 7500 cm^{-1}. In complete analogy to the case for the corresponding $Cu(terpy)_2X_2$ compounds[6] the existence of this band gives definite evidence for the presence of a lower symmetry ligand field component. It corresponds to the transition within the octahedral ^2E ground state ($\simeq 4E_{JT}$), which assignment is also strongly supported by EPR spectroscopy (see below). The interpretations of Co^{2+} spectra of this type up to now were based on the assumption of an (approximately) octahedral CoN_6 geometry[11] without the presence of a Jahn–Teller distortion and/or a geometric ligand effect. The ligand field parameter Δ_0 may be estimated by comparison with analogous Cu^{2+}– ($\Delta_0 \simeq 11\,500$ cm^{-1}) and Ni^{2+}–terpyridine complexes ($\Delta_0 \simeq 12\,500$ cm^{-1}).[6] Taking also into account reported data for octahedral Co^{2+} complexes with other nitrogen ligands,[11] we have assumed Δ_0 to be $\simeq (15 \pm 1) \times 10^3$ cm^{-1}. With the additional restriction that the lowest doublet and quartet states are very close in energy (compare the susceptibility data discussed below), the Racah parameters B and C can also be estimated. The chosen value of $B = 750$ cm^{-1} corresponds to a nephelauxetic ratio $B/B_0 = 0.76$ ($B_0 = 990$ cm^{-1}), which is intermediate between the values used for the low-spin $[Co(NO_2)_6]^{4-}$ and the high-spin $[Co(bpy)_3]^{2+}$ complexes.

Table II. Calculated Positions (in 10^3 cm^{-1}) and Relative Intensities of Ligand Field Bands for $Co(terpy)_2X_2 \cdot 1.5H_2O$ (C_{2v} Symmetry)[a]

term[b]	energy	I[c]	energy	I[c]
$^2A_1(a_1a_1'^2)$	7.5	$0.93p_z$	7.5	$0.93p_z$
$^2B_2(a_1a_1'b_2)$	12.4	$0.94p_x^a - 0.60p_x^b$	14.1	$0.96p_x^a - 0.58p_x^b$
$^2B_1(a_1a_1'b_1)$	14.1	$1.13p_y^a + 0.64p_y^b$	15.7	$1.15p_y^a + 0.62p_y^b$
$^2B_2(a_1a_1'b_2)$	16.1	$0.58p_x^a + 0.26p_x^b$	17.9	$0.56p_x^a + 0.27p_x^b$
$^2B_1(a_1{}^2b_1)$	17.4	$0.69p_y^a - 0.55p_y^b$	19.3	$0.68p_y^a - 0.57p_y^b$
$^2B_1(a_1a_1'b_1)$	17.7	$0.35p_x^a + 0.29p_x^b$		
$^2B_2(a_1a_1'b_2)$			19.5	$0.26p_x^a + 0.23p_x^b$
$^2B_2(a_1{}^2b_2)$	18.1	$0.68p_x^a + 0.53p_x^b$	20.0	$0.73p_x^a + 0.59p_x^b$

[a] $B = 740$ cm^{-1}, $C/B = 4.47$ and 5.5; $\Delta(^2E) = 13\,200$ and $15\,200$ cm^{-1}; $E_{JT} = 2000$ cm^{-1}; $\lambda = 440$ cm^{-1}; $\varphi_0 = 158°$. Δ energies and C/B ratios refer to columns 2, 3 and 4, 5, respectively. [b] The term designation corresponds to the most significant contribution to the respective function (d^3 hole configuration). [c] Relative intensities in terms of nonvanishing dipole transition elements polarized along the molecular z, x, and y axes (cf. Appendix).

The low-spin EPR data lead to an angular distortion parameter $\varphi_0 \simeq 158°$ (compare below), implying a strong orthorhombic distortion component. With $E_{JT}' \simeq 250$ cm^{-1}, derived below, a splitting of the octahedral t_2 states by the noncubic ligand field components of only $\simeq 700$ cm^{-1} results.

A ligand field calculation in the strong-field scheme with all configuration and spin–orbit interactions in the point group C_{2v} (theory in ref 15) was performed. It is based on the assumption that the maxima of the ligand field bands (4.2 K) are correlated with Franck–Condon transitions originating from the zero vibrational ground states.

The intensities increase slightly with decreasing temperature. Obviously the transitions are symmetry allowed as the consequence of the missing inversion center in the CoN_6 polyhedra and hence are of electric dipole origin. For a semiquantitative estimation of relative intensities the group theoretical selection rules in C_{2v} are used. The dipole transitions between the many electron states are generated from their one-electron components (Appendix). The calculated term energies and relative intensities listed in Table II are based on two alternative assignments and differ in the interpretation of the band at 19 200 cm^{-1} as d–d or charge-transfer transition, respectively. The uncertainties in the magnitudes of the ligand field parameters B, C, $\Delta_0(^2E)$, and E_{JT} as the consequence of the rather broad and unresolved ligand field bands are of only minor influence on the following discussion of the magnetic and EPR results. More detailed information with respect to band positions, intensities, and polarization behavior is expected from polarized single-crystal spectra.[16]

Magnetic Susceptibility Data. The effective magnetic moments $\mu_{eff} = 2.828(\chi_m^{cor}T)^{1/2}$ (experimental error $\approx \pm 0.05$ μ_B, temperature dependent) in units of μ_B are depicted as a function of temperature between 4.2 and 293 K in Figure 5. For all compounds with the exception of the ClO_4^- complex μ_{eff} decreases from 3 μ_B at 293 K to $\simeq 1.9 \pm 0.1$ μ_B at 4.2 K. Obviously these complexes possess a low-spin ground state with a magnetic moment close to the spin-only value of 1.8 μ_B. A sudden decrease of μ_{eff} when the temperature is lowered, which is often found for Fe^{2+} or Fe^{3+} compounds in the critical crossover region as a consequence of phase transitions,[17] is not observed for the Co^{2+}–terpyridine complexes studied. The temperature dependence of μ_{eff} seems to follow a normal Boltzmann distribution of electrons between energetically separated states of one molecule (see the Discussion). The ClO_4^- complex exhibits much larger μ_{eff} values with 4.2 μ_B at 293 K and $\simeq 3.5$ μ_B at 4.2 K, indicating predominantly high-spin-configured Co^{2+} ions even at 4.2 K in this case.

Table III. Single-Crystal g Values and Hyperfine Coupling Constants A (in cm^{-1}) for $Co(terpy)_2X_2 \cdot nH_2O$ Complexes

	low-spin			high-spin, $X = ClO_4^-$, $n = 0.5$, 4.2 K
	$X = NO_3^-$, $n = 0.5$, 77 K	$X = ClO_4^-$, $n = 0.5$		
		77 K[a]	4.2 K	
g_x	2.034	2.083	2.027	2.26 (10)
g_y	2.132	2.083	2.142	2.85 (10)
g_z	2.207	2.203	2.196	6.95 (5)
A_z	~0.008	0.0098	0.0098	0.0265
$A_x = A_y$	<0.001	<0.001	<0.001	<0.001

[a] $X = NO_3^-$, $n = 0.5$, and $X = Br^-$, $n = 3$, have nearly the same g tensors at 130 K.

The comparison of the magnetic moments of Figure 5 with those reported by other authors[10,11] shows pronounced differences, in particular for $X = Cl^-$ and ClO_4^-. We have studied this question more closely for the latter compound, which we prepared as single crystals and as powders of different grain sizes. The single crystals and the polycrystalline material contain half a molecule of water per formula unit and possess the tetragonal structure mentioned before.[2,3] If the water is extracted under reduced pressure (~ 50 torr), the structure of the single crystals is destroyed irreversibly. The polycrystalline samples indicate the existence of at least two phases but transform back into the tetragonal structure with $n = {}^1/_2$ when exposed to air of normal pressure.[22] Analogous structural changes occur if the compound with $n = {}^1/_2$ is thoroughly powdered. Thus, at least for the ClO_4^- complex, all measurements performed with powdered samples or after extraction of water are possibly not related to a unique phase. Though the essential features of the structure are most certainly not influenced by these procedures, finer details of the arrangement of the ionic constituents within the lattice are probably changed. The magnetic data sensitively depend on the high-spin/low-spin ratio and hence may considerably diverge for single crystals on the one hand and powdered material on the other.

EPR Spectra. EPR powder spectra (35 GHz) of the compounds investigated (X, n: Cl^-, 5; Cl^-, 1.5; Br^-, 3; I^-, 1.5; NO_3^-, 0.5; ClO_4^-, 0.5) exhibit only broad signals in the low-spin region at 298 K. They are tetragonal down to 130 K with $g_\perp \simeq 2.08$ and $g_\parallel \approx 2.2$. At temperatures $\lesssim 77$ K a distinct splitting of $g_\perp$ is observed leading to an orthorhombic symmetry pattern: $g_x = 2.03$ (1), $g_y = 2.12$ (1), and $g_z \simeq 2.20$. Clearly an exception is the ClO_4^- complex, which shows an EPR spectrum only below 130 K and an additional high-spin signal at 4.2 K.

Single-crystal data (35 or 9 GHz) in three mutually perpendicular planes were collected for $X = Br$, $n = 3$, $X = NO_3$, $n = 0.5$, and $X = ClO_4^-$, $n = 0.5$ (Table III). In analogy to the Cu^{2+} complexes, the **g** tensors are not exchange coupled but reflect the individual $[Co(terpy)_2]^{2+}$ units. Below 77 K a local orthorhombic symmetry is found in all crystals investigated. In the nitrate and perchlorate two sublattices are found, which are oriented perpendicular with respect to each other (antiferrodistortive order in the (001) plane). The principal g values are detected in the crystallographic [001] direction (g_z) and in the (001) plane (g_x, g_y) (crystal visually

(15) E. König and S. Kremer, "Ligand Field Energy Diagrams", Plenum Press, New York, 1977.
(16) M. Hitchman and S. Kremer, to be submitted for publication.
(17) P. Gütlich, *Struct. Bonding (Berlin)*, **44**, 83 (1981).
(18) H. Margenau and G. M. Murphy, "Die Mathematik für Physik und Chemie", H. Deutsch, Frankfurt, 1965.
(19) S. Sugano, Y. Tanabe, and H. Kamimura, "Multiplets of Transition Metal Ions in Crystals", Academic Press, New York, 1970.
(20) F. S. Ham, *Phys. Rev.*, **138**, 1727 (1965).
(21) J. Wajnflasz, *Phys. Status Solidi*, **40**, 537 (1970).
(22) U. Sondermann and S. Kremer, *Verhandl. DPG (VI)*, **17**, 824 (1982).

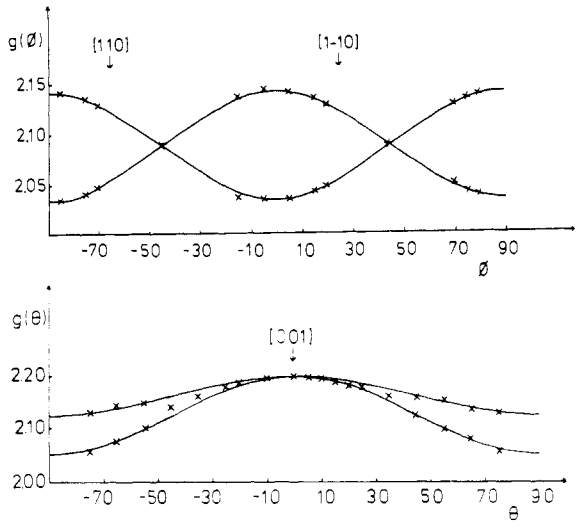

Figure 6. Angular dependence of the low-spin **g** tensor for Co(terpy)$_2$(ClO$_4$)$_2$·0.5H$_2$O in the crystallographic (001) and (110) planes (Φ and θ) (curves correspond to least-squares fits of experimental points).

oriented). While g_x and g_y follow the crystallographic axes in Co(terpy)$_2$(NO$_3$)$_2$·0.5H$_2$O, they enclose an angle of ~20° with the [010] and [100] directions, respectively, in the ClO$_4^-$ complex (Figure 6). This is exactly the angle between the molecular x, y directions and [100], [010] in the latter compound,[3] which is isomorphous with Cu(terpy)(NO$_3$)$_2$.[6]

The orthorhombic low-spin **g** tensor found below 77 K is explained in analogy to that for the Cu^{2+} complexes. The tetragonal compression along the molecular z axis, induced by the rigid ligands, is superimposed by a tetragonal elongation along x or y as the consequence of the Jahn–Teller effect. The Jahn–Teller symmetry component appears to be less pronounced compared to that for the Cu^{2+} complexes, however. The g values are in agreement with an angular distortion parameter φ_0 near 150°, for which the following first-order relations hold:

$$g_z = g_0 + (4 + 2(3^{1/2}))u \qquad g_{y(x)} = g_0 + 4u$$
$$g_{x(y)} = g_0 + (4 - 2(3^{1/2}))u \tag{11}$$

An orbital contribution of $u \approx 0.03$ yields $g_z \simeq 2.22$, $g_y \simeq 2.12$, and $g_x \simeq 2.02$, nearly in accord with the experimental values in Table III. The tetragonal **g** tensor at higher temperatures indicates a transition to the dynamic Jahn–Teller effect. The different Co–N bond lengths in the molecular x and y directions equilibrate dynamically. The corresponding motional narrowing of g_x and g_y to $g_\perp = 2.07$ is thus experimentally established.

The well-resolved hyperfine structure of eight lines in the signal of the ClO$_4^-$ complex (77 K) parallel to [001] agrees with the nuclear moment $I = {}^7/_2$ of ^{57}Co. The hyperfine splitting constant is $A_\parallel \approx 98 \times 10^{-4}$ cm^{-1} ($\Delta H_{pp} \simeq 140$ G). No splitting due to hyperfine interactions is observed in the (001) plane, however, implying an $A_\perp$ value smaller than 10×10^{-4} cm^{-1}. At 4.2 K the hyperfine structure due to $A_\parallel$ is not resolved any more, though the line shape still indicates its presence. From a line-shape calculation (eight Lorentzian curves) the same $A_\parallel$ value as observed at 77 K results. We think that the disappearance of the hyperfine structure is due to the superposition of two resonance lines shifted in phase by ~20–40 G. This is supported by the somewhat larger half line width (≃145 G) measured at 4.2 K. The reason is possibly that the two Co^{2+} sites that constitute the antiferrodistortive order become slightly different in the molecular $g_\parallel$ values in going from 77 to 4.2 K (compare high-spin results below). In the case of X = NO$_3^-$, $n = 0.5$, the hyperfine

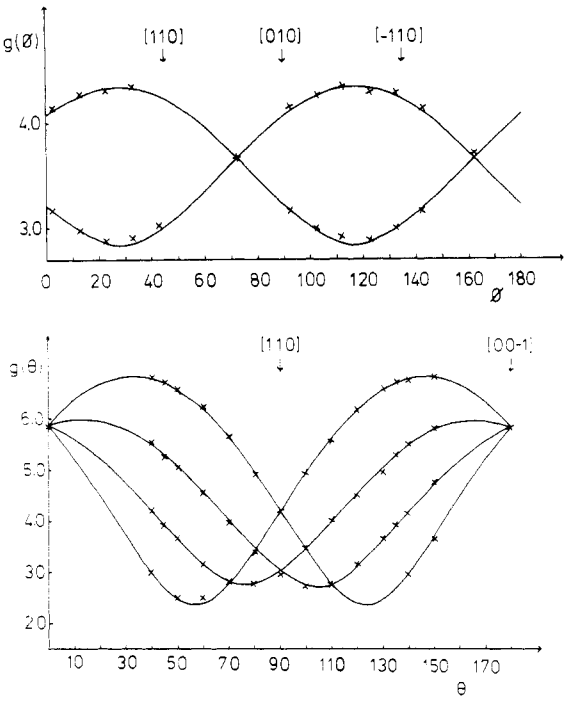

Figure 7. Angular dependence of the high-spin **g** tensor for Co(terpy)$_2$(ClO$_4$)$_2$·0.5H$_2$O in the crystallographic (001) and (110) planes (Φ and θ) (curves correspond to least-squares fits of experimental points).

splitting is not well resolved; a coupling constant of $A_\parallel \approx 8 \times 10^{-3}$ cm^{-1} is estimated by line-shape calculation.

In addition to the low-spin EPR spectra, which are almost equivalent for all Co^{2+} complexes investigated, high-spin signals are present in the case of the ClO$_4^-$ complex at 4.2 K. Q-Band measurements (35 GHz) with powder samples of the ClO$_4^-$ compound yielded $g_z \simeq 6.7$ (1) and $g_{x,y} \simeq 2.8$ (2) ($\Delta H_{pp} \approx 1100$ G). Four single crystals, mounted on a LiF crystal with a possible misorientation of ±5°, were investigated by rotating the external magnetic field in the (110), (1,−1,0), and (001) planes at 4.2 K. In the [001] direction a sharp signal at $g = 5.85$ (3) ($\Delta H_{pp} = 165$ G) is observed with an unresolved hyperfine structure and a coupling constant A of the same magnitude as found under X-band conditions (see below). In the (110) and (1,−1,0) planes up to four signals appear with the largest and lowest g values near to those of the powder samples (Figure 7). Though the intensity and line width vary widely with the field direction, the planes (110) and (1,−1,0) can be considered to be equivalent within the experimental error. The angular dependence within the (001) plane is determined by only two signals (Figure 7). The line widths and intensities of the EPR signals in specific planes differ appreciably from crystal to crystal. While, for example, comparatively sharp signals ($\Delta H_{pp} = 150$–250 G) were observed in all directions for one of the crystals, the line width increased in the case of the other three crystals ($\Delta H_{pp} \approx$ 1000–1500 G), if the field direction deviated from [001] and (001). The different line width variations for the various crystals may be connected with order–disorder phenomena between the high- and low-spin Co^{2+} ions in the lattice, as mentioned before. From the angular dependence of the EPR signals the g values $g_{z'} = 6.95$ (2), $g_{y'} = 2.84$ (10), and $g_{x'} = 2.26$ (10) are derived. The direction of the **g** tensor is related to the crystal axes a, b, and c by the transformation

$$(x' \quad y' \quad z') = R(\alpha\beta\gamma)\begin{pmatrix} a \\ b \\ c \end{pmatrix} \tag{12}$$

with the Euler angles defined in the usual way by $R(\alpha\beta\gamma) =$

Table IV. Euler Angles for the Rotation of Molecular High-Spin g Tensors of Center *i* into the Crystal Axes for $Co(terpy)_2(ClO_4)_2 \cdot 0.5H_2O$ (Compare Text and Figure 8)

i	α	β	γ	*i*	α	β	γ
1	26.6	34.5	−93.3	3	116.6	34.4	−93.3
2	26.6	−34.4	−93.3	4	116.6	−34.4	−93.3

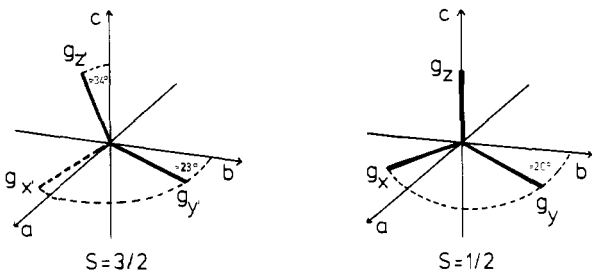

Figure 8. Orientations of molecular **g** tensors g_x, g_y, g_z in relation to the crystal axes *a*, *b*, *c* for high-spin and low-spin Co^{2+} (cf. Figures 6 and 7; for $S = {}^3/_2$ $g_{x'}$ deviates from the (001) plane in the [001] direction; the correlation to the molecular axes *x*, *y*, *z* is discussed in the text).

$R_c(\gamma) \cdot R_{c'}(\beta) \cdot R_c(\alpha)$.[18] Four magnetically nonequivalent Co^{2+} sites result, with the Euler angles of Table IV. $g_{y'}$ ($=g_y$) forms an angle of ~23° (±5°) with the *a* or *b* axis, while $g_{z'}$ deviates from the *c* axis by 34° (Figure 8). The orientation of the observed **g** tensor (*x'*, *y'*, *z'*) implies that the high-spin $Co(terpy)_2^{2+}$ ions do not possess a C_2 axis parallel to [001]. Obviously the space group $I4_1/a$ of the room-temperature phase[3] is not retained at 4.2 K. The symmetry reduction of the Co^{2+} sites from C_{2v} to C_s is presumably caused by a rotation of the three nitrogen ligands of one ring in the *xz* plane with respect to the molecular frame in Figure 1. As will be demonstrated in the Discussion a small rotation of this kind is sufficient to explain the large orientational change in the **g** tensor. An effect of this magnitude on the **g** tensor is indeed expected, if the considerable orbital contributions to the d_{yz} ground state are considered. Because orbital contributions are small in the case of low-spin Co^{2+} ions, the orientation of the corresponding **g** tensor should not be influenced to a larger extent—in agreement with the experimental evidence. A deviation of the N ligands from the molecular axes in the way just mentioned, which is not observed in the room-temperature structure of $Co(terpy)(ClO_4)_2 \cdot {}^1/_2H_2O$,[3] is found in triclinic $Co(terpy)_2Br_2 \cdot 3H_2O$ at 298 K.[1] The occurrence of four differently orientated **g** tensors is probably due to a two-domain structure. These two domains, each of which induces two signals, are related to each other by a mirror plane containing the molecular *z* and *y* axes (Figures 1 and 8). The two signals of each domain originate from two sublattices, which constitute an antiferrodistortive order with different Co–N bond lengths in the (001) plane—in the same way as for the low-spin CoN_6 polyhedra. After all, the orientations of the molecular axes are not necessarily different for high- and low-spin Co^{2+}. Furthermore, the hyperfine structure along [001] is wiped out in the same way as in the case of low-spin Co^{2+} and presumably caused by an analogous reason.

The angular dependence of the **g** tensor in the (001) plane observed under X-band conditions is identical with the one in Figure 7. Because of the large hyperfine splitting in the [001] direction ($A_z = 265 \times 10^{-4}$ cm^{-1}; line shape calculated with $\Delta H_{pp} = 160$ G) the four-line structure between (001) and [001] could not be resolved, however.

Discussion

Models. Two models are suitable to explain the experimental results in spin-mixed systems. The first implies a thermal spin equilibrium with intramolecular electronic transitions between different states. In the second model the possible occupation of different sites in the lattice by either high-spin or low-spin ions, both with energetically well-separated excited states of different spin ($E_{42} >> kT$), is considered. In both cases the Zeeman splitting calculations are performed in the ligand field model with the complete d^7 basis set in the point group C_{2v}. Explicitly the parameters of eq 9 are derived from the ligand field spectra (*B* and *C* are assumed to be equal for doublet and quartet states—$\Delta_0(^2E)$, $E_{JT}(^2E)$) and the EPR results ($E_{JT}'(^4T_1)$, φ_0^*, φ_0'; eq 5 and 5a). The quartet–doublet separation—and hence $\Delta_0(^4T_1)$—can be obtained additionally from the susceptibility data in the case of the first model. The orbital reduction factors κ in the Zeeman operator

$$H_m = \mu_B/\hbar \sum_i^7 (\kappa_{\parallel} \cdot \mathbf{l}_{iz} + 2\mathbf{s}_{iz}) + \kappa_{\perp}(\mathbf{l}_{ix} + \mathbf{l}_{iy}) + 2(\mathbf{s}_{ix} + \mathbf{s}_{iy})$$

and the effective spin–orbit coupling constants $\zeta_{\parallel}$ and $\zeta_{\perp}$ in the expansion of the (**s**·**l**) operator

$$H_{SO} = \sum_i^7 [\zeta_{\parallel}(r)](\mathbf{s}_{iz} \cdot \mathbf{l}_{iz}) + [\zeta_{\perp}(r)]((\mathbf{s}_{ix} \cdot \mathbf{l}_{ix}) + (\mathbf{s}_{iy} \cdot \mathbf{l}_{iy}))$$

are treated as semiempirical variables in order to give best agreement with the experimental *g* factors and magnetic moments. Although different reduction factors in Zeeman and spin–orbit operators follow from fundamental MO considerations,[19] a conversion corresponding to $\zeta_i = \kappa_i \zeta_0$ ($i = \perp, \parallel$; $\zeta_0 = 515$ cm^{-1}) was introduced.

In the case of a thermal spin equilibrium the effective average magnetic moments are calculated on the basis of a Boltzmann distribution of electrons over the ground-state multiplet originating from the octahedral ^2E and $^4T_1$ states. The calculated μ_{eff} vs. *T* dependencies are given in Figure 5 as full curves. The energy separation E_{42} is considered as a temperature-independent parameter. As the ligand field spectra and **g** tensors do not depend significantly on X and *n*, the geometries of the CoN_6 entities in the different compounds are considered to be essentially equal. As illustrated by the adiabatic potentials in Figure 3, an electron transition from the doublet to a quartet state can occur by thermal excitation in the geometry ρ_0 with a subsequent relaxation into a quartet ground state with the distortion ρ_0'.

Different energy separations $E_{42} \simeq 0$–500 cm^{-1} follow from the susceptibility data. They should induce largely varying **g** tensors, if the ligand field model mentioned above is applied. Because this contradicts the observation of nearly identical low-spin *g* values for the different compounds, the spin–orbit coupling between doublet and quartet states is obviously largely quenched. This might be caused by the reduced overlap[20] of the vibronic functions, which are connected with the two electronic spin states. The reduction can be attributed to the difference in the distortion parameters (ϵ vibrational mode) and most certainly to the different average Co–N bond length (a_1 vibrational mode) for low- and high-spin Co^{2+} also. The "ρ effect" should be of the magnitude $[\exp(-\mu\omega_\epsilon^2(\rho_0 - \rho_0')^2/4\hbar\omega_\epsilon)]^2$ ($\omega_\epsilon \simeq \omega_\epsilon'$). After all, the ground state is of pure doublet character with no significant quartet contribution mixed in. Hence the adiabatic potentials are not disturbed by each other. Transitions between the two minima cannot be induced by phonon excitation alone but most likely occur via combined electron–phonon excitations. As the low-spin *g* factors do not shift to higher values with increasing temperature, the lifetime of the excited quartet states must be larger than 10^{-8} s. Otherwise averaged *g* values of high-spin and low-spin states are expected and observed, for example, in the Ni^{3+} compounds $A_2A'NiF_6$.[5,13]

The model of thermal spin equilibrium described above is in agreement with all experimental results. The μ_{eff} vs. *T* curves are well reproduced by a Boltzmann distribution with

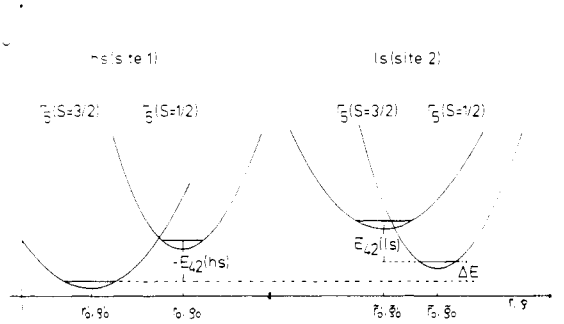

Figure 9. Adiabatic potentials of high-spin and low-spin Co^{2+} (lowest two Kramers doublets only), depicting the cooperative model of spin exchange.

temperature-independent energy separations E_{42}. In accord with the observation of EPR signals for high- and low-spin Co^{2+} side by side at 4.2 K the corresponding zero phonon states are of nearly equal energy in the ClO_4^- complex. The other compounds are characterized by high-spin–low-spin separations between 300 and 500 cm^{-1}. The inclusion of nonzero vibrational states in addition to the zero phonon states should change the energy separation only if the energies of the zero-point motions in the two states are smaller than E_{42}. In any case the influence of nonzero vibrational states on E_{42} is negligible if only low-temperature results are used.

Another possibility that explains the experimental results is the assumption that different lattice sites are occupied by Co^{2+} ions with either high-spin or low-spin ground states. With the exception of X = ClO_4^-, the observed temperature dependence of μ_{eff} (Figure 5) then leads to a high-spin/low-spin ratio γ, which varies from $\gamma \simeq 0.4$ at 300 K to $\gamma \simeq 0$ at 4.2 K. For X = ClO_4^- the calculated μ_{eff} vs. T curves can be adapted to the experiment by

$$\mu_{eff}^2 = \alpha[\mu_{eff}(hs)]^2 + (1 - \alpha)[\mu_{eff}(ls)]^2$$

with $\alpha \simeq 0.7$ ($\gamma \simeq 2.3$) for the whole temperature range. This number is in good agreement with the intensity ratio of the high-spin and low-spin EPR signals: $I(hs)/I(ls) \simeq 2.0$, which is $\alpha \simeq 0.6_7$ for all crystals investigated.

In contrast to the model discussed above, which contains thermal excitations on *one* Co^{2+} site, the second model is clearly *cooperative*. Restricting ourselves to pairs of interacting Co^{2+} ions on sites 1 and 2 in a simplified picture, the spin transition mechanism can be formulated as

$$\text{hs(site 1)} + \text{ls(site 2)} \rightleftharpoons \text{ls(site 1)} + \text{hs(site 2)} \quad (13)$$

In Figure 9 the adiabatic potentials of these high-spin and low-spin sites are depicted, which have different equilibrium positions r_0 and ρ_0 with respect to the a_1 and ϵ modes. The excited spin states are well separated from the respective ground states in this model, however ($E_{42}(hs)$, $E_{42}(ls) >> kT$, ΔE), in agreement with the observation of low-spin g parameters independent of X and n. With neglect of entropy contributions the concentration ratio γ of high-spin and low-spin Co^{2+} is controlled by the energy difference ΔE in Figure 9. The activation energy, which determines the spin transition rate in site 1 or 2, is probably connected with the energies $E_{42}(hs)$ and $E_{42}(ls)$. The sketched transition mechanism resembles closely the one of Wajnflasz.[17,21] A decision for one of the two spin conversion mechanisms is not possible from the presently available experimental data. In particular the direct spectroscopic determination of the quartet–doublet separation E_{42} and the knowledge of the lifetimes of the excited states are necessary. In addition a more complete theoretical treatment has to include the coupling of the electronic states to the lattice phonons. Some evidence for the cooperative mechanism is the antiferrodistortive order observed for low-spin and high-spin Co^{2+} as well. Obviously significant intermolecular elastic interactions are present, which may have an influence on the magnitude of E_{42} also. In the following section the bonding and geometry of the CoN_6 polyhedra are discussed.

Table V. g Values and Ligand Field and Distortion Parameters (in 10^3 cm^{-1}) Calculated from Experimental Data for the Compounds $Co(terpy)_2X_2 \cdot nH_2O$ (C_{2v} Symmetry, Including ($S \cdot L$) Coupling ($\lambda_0 = 515$ cm^{-1}), 4.2 K)

$S = {}^1/_2$

$g_{x(y)}$	$g_{y(x)}$	g_z	Δ_0	E_{JT}	E_{JT}' [a]
2.02	2.12	2.21	15.2	2.0	0.3

ρ_0, pm	φ_0, deg	$k_\parallel$	$k_\perp$	V_ϵ, cm^{-1} pm^{-1}	$M\omega_\epsilon^2$, cm^{-1} pm^{-2}
26	158, 202	0.8	0.9	150	5.7

e_σ^x	e_σ^y	e_σ^z	$e_\pi^{x\,a}$	$e_\pi^{y\,a}$	$e_\pi^{z\,a}$
6.1	7.7	10.4	1.6	2.4	4.4

$S = {}^3/_2$

g_x	g_y	g_z	Δ_0 [a]	E_{JT}'	ρ_0', pm
2.32	2.86	6.91	13.5	0.25	14

φ_0', deg [b]	e_π^{xy}	e_π^z	V_ϵ', cm^{-1} pm^{-1}	$M\omega_\epsilon'^2$, cm^{-1} pm^{-2}
166, 194	0.6	0.95	35	2.5

[a] Estimated from AOM calculations. [b] Calculated from g tensors with isotropic orbital reduction ($k_\parallel \simeq k_\perp \simeq 0.9$).

The Low-Spin State. From the low-spin g factors at 4.2 K an angular parameter $\varphi_0 = 158°$ (202°) can be calculated. Taking this value and using the Co–N bond lengths $a_z = 189$ pm and $\bar{a} = 203$ pm from the room-temperature structure of $Co(terpy)_2Br_2 \cdot 3H_2O$,[1] we obtain $a_{x(y)} = 214._5$ pm, $a_{y(x)} = 205._5$ pm, and a radial distortion parameter $\rho_0 = 26$ pm. The reader is referred to eq 19 and 5 in ref 5 to reproduce these results. In comparison to those for $Cu(terpy)_2(NO_3)_2$ ($a_x = 229$ pm, $a_y = 208$ pm, $a_z = 199.5$ pm, from ref 4 and Table I) the Jahn–Teller distortion component, which superimposes the ligand effect, is less significant. This is clearly indicated by the smaller ρ_0 and larger φ_0 values (Table V). At temperatures $T \gtrsim 77$ K the Jahn–Teller distortion component becomes dynamic. The **g** tensor changes from orthorhombic to tetragonal, in agreement with equilibrated Co–N bond lengths $a_x \simeq a_y = 210 \pm 1$ pm (Figure 1) in the structure mentioned above.[1] A similar change was observed for $Cu(terpy)_2Br_2 \cdot 3H_2O$[4]—in contrast to the case of the nitrate complex with a static Jahn–Teller distortion of the CuN_6 polyhedra even at 298 K.

The average Co–N and Cu–N bond lengths in the bromide compounds[1,4] are 203 and 211 pm, respectively. The ionic radii[12] of Cu^{2+} (73 pm) and low-spin Co^{2+} (65 pm) show the same difference, in satisfactory agreement with the magnetic result of only small high-spin contributions in the room-temperature structure of the Co^{2+} complex.

If (in analogy to the case for Cu^{2+}) the total distortion effect is considered to be of vibronic origin, a linear vibronic coupling constant $V_\epsilon(^2E) \simeq 150$ cm^{-1} pm^{-1} results from the lowest energy ligand field band (eq 3). The force constant of the radial ϵ vibration is $M\omega_\epsilon^2 = 5.7$ cm^{-1} pm^{-2}. Again with $M = 78/N_L$ g a zero-point energy of 165 cm^{-1} results, which is significantly larger than the one (120 cm^{-1}) for the longer Cu–N bond.

For the calculation of the bonding parameters in the AOM description the same approach and the same angular deviations of the N ligands from the equatorial plane (Figure 1) as described for Cu^{2+} were used. With the ground-state splitting

of 7500 cm^{-1} and the Co–N bond lengths derived from the **g** tensor at 4.2 K a K_σ parameter of 1.14×10^6 cm^{-1} was calculated from eq 4. Atomic functions of $Co^{2+}(3d)$ and $N^0(2p)$[9] were used to calculate the overlap integrals. With use of the octahedral ligand field parameter $\Delta_0(^2E) \simeq 15000$ cm^{-1}, estimated from the electronic spectra, a K_π value of $\simeq 1.0 \times 10^6$ cm^{-1} results from eq 4a and 7. The obtained e_σ and e_π energies (Table V) show similar trends compared to those of Cu^{2+} (Table I) but are larger in the average by a factor of about 1.5. The considerable increase of the e_i energies going from Cu^{2+} to Co^{2+} is obviously a consequence of the smaller Co–N bond length on the one hand and a comparatively stronger Co–N covalency on the other. The latter argument follows from the observation that equal bond lengths induce e_i energies larger for Co^{2+} than for Cu^{2+}. Similar changes in the magnitudes of the discussed energy parameters are observed for nitro complexes also, when Cu^{2+} and Co^{2+} are compared.[5]

The High-Spin State. The structure determination of $Co(terpy)_2(ClO_4)_2 \cdot 0.5H_2O$[3] yields an average Co–N bond length of 210 pm, which is slightly less than the one expected for the high-spin configuration ($r(Co^{2+},hs) = 65$ pm, $r(Co^{2+},ls) = 73.5$ ppm;[12] $\bar{a}(Co[1s]-N) = 203$ pm). This finding is in qualitative agreement with the presence of about 30% low-spin Co^{2+} in this compound at 298 K. The structural identification of low-spin and high-spin Co^{2+} ions in the case of complete disorder is hardly possible, not even by an analysis of the temperature ellipsoids of Co^{2+} and N. If the high-spin/low-spin ratio is 1, the temperature factors U_{ij} would change only by about 10% compared to those of the pure high- or low-spin compounds. In terpyridine complexes of the type investigated the U_{ij} parameters are not determined with the precision necessary to detect an effect of this kind, however.

Provided the AOM parameters e_i reflect changes in metal to ligand bonding dependent on the bond lengths, the K_i values should be identical for high- and low-spin Co^{2+}. With the Co–N distances in the perchlorate complex at 298 K ($a_x = a_y = 214$ pm, $a_z = 202$ pm; $\rho_0(^4T_1) \equiv \rho_0' \simeq 14$ pm) we obtain $e_\sigma^{xy} = 6300$ cm^{-1}, $e_\sigma^{z} = 8200$ cm^{-1} and $e_\pi^{xy} = 1700$ cm^{-1}, $e_\pi^{z} = 2700$ cm^{-1}. The Jahn–Teller splitting of the excited ^2E ($t_2^6e^1$) state at ρ_0' (Figure 9, site 1) is then calculated to be $4E_{JT} = 2V_e\rho_0' \simeq 4200$ cm^{-1}. A ligand field calculation yields values of $\Delta(^4T_1) \simeq 13500$ cm^{-1} and $E_{42} \simeq -3500$ cm^{-1}, for the octahedral ligand field parameter of high-spin Co^{2+} and the high-spin–low-spin separation (vertical Franck–Condon transition), respectively.

The splitting of the one-electron t_2 orbital is sensitively reflected by the **g** tensor and calculated to be $E(xz,yz) - E(xy) \equiv 3E_{JT}' \simeq 700$ cm^{-1}. The AOM parameters $K_\pi \simeq 0.36 \times 10^6$ cm^{-1}, $e_\pi^{xy} = 600$ cm^{-1}, and $e_\pi^{z} \simeq 950$ cm^{-1}, derived from E_{JT}', are considerably smaller than those based on the low-spin data, however. Though the anisotropy in $g_\perp$ ($g_x \neq g_y$) clearly indicates an orthorhombic distortion component in the CoN_6 polyhedra at 4.2 K, values for φ_0' and the Co–N bond lengths (in analogy to those for Cu^{2+} and low-spin Co^{2+} as discussed above) can only be roughly estimated because of the large number of intercorrelated parameters. In any case the anisotropy of the Co–N bond lengths in the molecular xy plane should not exceed $a_x - a_y \simeq 4$ pm ($|\varphi_0' - 180°| \lesssim 15°$) in the low-temperature phase. From the splitting of the t_2 orbitals $3E_{JT}' = 700$ cm^{-1}, vibronic parameters $V_\epsilon' \simeq 3.5$ cm^{-1} pm^{-1}, $M\omega_\epsilon'^2 = 2.5$ cm^{-1} pm^{-2}, and $\hbar\omega_\epsilon' \simeq 108$ cm^{-1} are estimated for the $^4T_1$ state. Obviously the Jahn–Teller stabilization, if present at all, is smaller by a factor of about 10 compared to E_{JT} in the ^2E ground state and comparable in magnitude to the spin–orbit coupling (Table V). As also no quenching of orbital angular momentum in the high-spin configuration is observed, the ground-state stabilization should be predominantly attributed to spin–orbit coupling and the steric ligand effect. The Jahn–Teller influence is small as expected, because the display of spin–orbit coupling against vibronic interaction seems to be a general property of high-spin Co^{2+} complexes.[20]

Finally some comments concerning the direction of the high-spin **g** tensor with respect to the molecular frame of the CoN_6 entity seem necessary. Although low-temperature structural data for $X = ClO_4^-$ are not available, the assumption of a local symmetry lower than C_{2v}, found at 300 K,[3] is surely reasonable. A symmetry lowering of this kind is found for X = Br, $n = 3$, already at 300 K. A rotation of one tridentate ligand with respect to the other around the molecular y direction by only $\simeq 3°$ (Figure 1), leading to the point group C_s, induces in the AO model a nondiagonal matrix element $\langle d_{xy}|V_{LF}|d_{xz}\rangle \simeq 200$ cm^{-1}. While this perturbation has practically no influence on the *low-spin* **g** tensor, it causes a rotation of the *high-spin* $g_{x'}$ and $g_{z'}$ directions around y by $\simeq 17°$ (calculation with complete d^7 basis set) (Figure 8). Though the experimental value is $\simeq 34°$, an effect of the described kind is presumably responsible for the different directional behavior of the high- and low-spin **g** tensors.

Summary

The compounds $Co^{II}(terpy)X_2 \cdot nH_2O$ were investigated by optical and EPR spectroscopy, structural methods, and magnetic susceptibility measurements, in particular to study the high-spin–low-spin behavior. With the exception of $X = ClO_4^-$, $n = 0.5$, a pronounced temperature dependence of the magnetic moments was detected, with ~30% high-spin contribution at 300 K and a pure low-spin ground state at 4.2 K. For all compounds low-spin EPR signals corresponding to an octahedral $^2A_1(^2E)$ state of σ-antibonding character (C_{2v}) were observed. The Jahn–Teller splitting of the ^2E state is $4E_{JT} \simeq 8000$ cm^{-1} and the radial and angular distortion parameters are $\rho_0 \simeq 26$ pm and $\varphi_0 \simeq 158°$, respectively. In analogy to the case for the isostructural Cu^{2+} complexes the tetragonal compression along the z axis induced by the rigid ligands is superimposed by a tetragonal elongation along the molecular x or y axis as the consequence of a strong Jahn–Teller effect. While the Jahn–Teller distortion is dynamic at $T \gtrsim 77$ K, yielding a tetragonal **g** tensor by the thermal equilibration of the Co–N bond lengths in the equatorial plane, it becomes static with an orthorhombic **g** tensor at low temperatures. In the cases investigated the CoN_6 polyhedra exhibit an antiferrodistortive order pattern in the (001) plane of the unit cell. For $X = ClO_4^-$ only a weak temperature dependence of the magnetic moments was found with about 60% high-spin character in the whole temperature range. For this compound high-spin **g** factors could be observed and analyzed at 4.2 K, in addition to the low-spin EPR signals. The high-spin ground state seems to be stabilized nearly exclusively by spin–orbit coupling and the steric effect of the rigid ligands. The additional Jahn–Teller effect is only very weak and hence the CoN_6 polyhedron only moderately distorted (estimated parameters: $3E_{JT} \approx 700$ cm^{-1}; $\rho_0' \approx 14$ pm; $\varphi_0' \approx 166°$).

The nature of the spin-exchange mechanism is not completely clear. A local, intramolecular mechanism of thermal spin equilibrium and an intermolecular, cooperative model are equally appropriate to explain the experimental results. The second model of disorder proposes Co^{2+} sites in the unit cell, which have either high-spin or low-spin ground states and thermally nonaccessible excited states of alternative spin. It seems more reasonable than the first one, because the EPR evidence of *two* spin states with comparable population in $Co(terpy)_2(ClO_4)_2 \cdot {}^1/_2H_2O$ has a simple explanation only in the cooperative model.

Appendix

The relative intensities of the ligand field bands can be approximated by the reduction of the many-electron matrix

elements of the electric dipole operator p^k ($k = x, y, z$) to the one-electron matrix elements according to

$$I_r(\Delta E) \simeq \Delta E|\langle (E_0)\Gamma\gamma|p^k|(E_n)\Gamma'\gamma'\rangle|^2 = \Delta E|\sum A\langle \Gamma_1\gamma_1|p^k|\Gamma_2\gamma_2\rangle|^2$$

$|(E_0)\Gamma\gamma\rangle$ and $|(E_n)\Gamma'\gamma'\rangle$ are the ground- and excited-state wavefunctions of energies E_0 and E_n, respectively, with $\Delta E = E_n - E_0$, whereas A is a function of several group-theoretical coefficients and of nonvanishing one-electron dipole transition elements $\langle \Gamma_1\gamma_1|p^k|\Gamma_2\gamma_2\rangle$.[19]

In the d^7 configuration with a doublet ground state in the symmetry C_{2v} only the transition elements

$$p_z = \langle a_1(d_{z^2})|p^z|a_1(d_{x^2-y^2})\rangle$$

$$p_y^a = \langle a_1(d_{z^2})|p^y|b_2(d_{yz})\rangle \qquad p_y^b = \langle a_1(d_{x^2-y^2})|p^y|b_2(d_{yz})\rangle$$

$$p_x^a = \langle a_1(d_{z^2})|p^x|b_1(d_{xz})\rangle \qquad p_x^b = \langle a_1(d_{x^2-y^2})|p^x|b_1(d_{xz})\rangle$$

are nonvanishing and can be treated as parameters. The d functions in braces designate the main contribution to the relevant MO. In Table II the nonvanishing coefficients A are given for the different transitions calculated with a complete d^7 basis set in C_{2v} symmetry and strong-field coupling.[15] For the reduction of the number of parameters and for an estimate of relative intensities an SCCC calculation was performed for the CoN_6 polyhedra resulting in the relations

$$p_y^a \simeq 1.2p_y^b \qquad p_x^a \simeq -0.6p_x^b \qquad p_y^a = 1.6p_x^a$$

Atomic functions of $Co^+(3d, 4s, 4p)$ and $N(2p)$[9] were used without considering in-plane Co–N bonding. The overlap charges were partitioned according to Rein et al.[23] and based on the structural data, which were deduced from the available experimental results, in particular at low temperatures (compare the section in the Discussion concerning the low-spin state). The relations between the $p_k^{a,b}$ parameters are strongly dependent on the N–Co–N angles and the Co–N bond distances. Only a minor influence of the kind of approximation used for the calculation of the nondiagonal elements $\beta_{\mu\gamma}$ was found and thus justifies the neglect of the influence of the C atoms.

The relative intensities of the two transitions $^2A_1(a_1{}^2a_1) \rightarrow {}^2B_2(a_1a_1'b_2)$ and $^2B_1(a_1a_1'b_1)$ are calculated to be about 1 order of magnitude larger than the other ligand field bands. Hence it seems questionable whether the observed peaks at 17 800 and 19 200 cm^{-1} originate from d–d transitions. The intensity of the band at 7500 cm^{-1} mainly depends on the difference between the two axial Co–N bond lengths. This transition is extremely weak in the solution spectra and probably indicates a more regular $Co(terpy)_2{}^{2+}$ geometry than is observed in the solid compound. A similar decrease in the intensity of this transition is found for the corresponding $Cu(terpy)_2{}^{2+}$ ion, if one compares the reflection with the solution spectra.

(23) R. Rein, G. A. Clarke, and F. E. Harris, "Quantum Aspects of Heterocyclic Compounds in Chemistry and Biochemistry", Vol. II, Israel Academy of Sciences and Humanities, Jerusalem, 1970.

Contribution from the Institut für Physikalische und Theoretische Chemie and the Physikalisches Institut, Abt. II, University of Erlangen-Nürnberg, D-8520 Erlangen, West Germany, and the Department of Chemistry, The Queen's University of Belfast, Belfast BT9 5AG, Northern Ireland

The High-Spin ($^5T_2$) ⇌ Low-Spin ($^1A_1$) Transition in Solid Tris(2,2′-bi-2-imidazoline)iron(II) Diperchlorate. Hysteresis Effects, Simultaneous Change of Spin and Lattice Characteristics, and Order–Disorder Phenomena of the Perchlorate Anion

E. KÖNIG,*[1a] G. RITTER,[1a] S. K. KULSHRESHTHA,[1a,b] and S. M. NELSON[1c]

Received November 6, 1981

The sharp high-spin ($S = 2$; $^5T_2$) ⇌ low-spin ($S = 0$; $^1A_1$) transformation in solid $[Fe(bi)_3](ClO_4)_2$ (bi = 2,2′-bi-2-imidazoline) has been shown by variable-temperature ^{57}Fe Mössbauer-effect and X-ray diffraction measurements to be essentially of first order. The ground states involved are characterized, at the transition temperature $T_c\uparrow$, by $\Delta E_Q{}^I(^5T_2) = 2.42$ mm s^{-1}, $\Delta E_Q{}^{II}(^5T_2) = 1.99$ mm s^{-1}, $\delta^{IS}(^5T_2) = +1.09$ mm s^{-1} and $\Delta E_Q(^1A_1) = 0.22$ mm s^{-1}, $\delta^{IS}(^1A_1) = 0.42$ mm s^{-1}. A pronounced hysteresis of $\Delta T_c = 6.5$ K has been observed, the transition being centered at $T_c\uparrow = 114.8$ K for rising and at $T_c\downarrow = 108.3$ K for lowering temperature. The Debye–Waller factor shows a decrease of $\Delta f \approx 14\%$ at T_c, the temperature dependence of the effective thickness $t_{^5T_2}$ and $t_{^1A_1}$ being well reproduced within the high-temperature approximation of the Debye model ($\Theta_{^5T_2} = 133$ K for $T < 180$ K, $\Theta_{^5T_2} = 106$ K for $T > 200$ K; $\Theta_{^1A_1} = 190$ K; $M_{Fe} = 57$ au). The X-ray diffraction patterns for the $^5T_2$ and $^1A_1$ phases show characteristic differences. The Mössbauer spectra of the $^5T_2$ phase exhibit two doublets of almost equal intensity and different ΔE_Q values. At $T_2{}^{ClO_4} \approx 199$ K, a transformation into a single $^5T_2$ doublet ($\Delta E_Q = 1.70$ mm s^{-1} and $\delta^{IS} = +1.04$ mm s^{-1} at $T_c{}^{ClO_4}$) is observed. Changes of X-ray diffraction patterns suuggest a first-order character of the transition. The phenomenon is attributed to an order–disorder transition of the ClO_4 anion which will result in changes of the iron–nitrogen ligation. The two crystallographically inequivalent iron sites below $T_c{}^{ClO_4}$ correspond thus to two possible configurations of the ClO_4 anions.

Introduction

Temperature-induced high-spin ⇌ low-spin transitions in certain complexes of d^5, d^6, d^7, and d^8 transition-metal ions are well documented.[2] In solution, the spin interconversion process is dynamic in nature, and its mechanism seems to be

(1) (a) University of Erlangen-Nürnberg. (b) On leave of absence from Bhabha Atomic Research Center, Bombay, India. (c) Queen's University of Belfast.

(2) (a) For most recent reviews, see: H. A. Goodwin, *Coord. Chem. Rev.*, **18**, 293 (1976); (b) E. König, *Ber. Bunsenges. Phys. Chem.*, **76**, 975 (1972); (c) R. L. Martin and A. H. White, *Transition Met. Chem (N.Y.)*, **4**, 113 (1968); (d) P. Gütlich, *Struct. Bonding (Berlin)*, **44**, 83 (1981).

0020-1669/82/1321-3022$01.25/0